Journal of Science and Transport Technology
Journal homepage: https://jstt.vn/index.php/en

Numerical study on the effect of ECC on shear behaviour of steel-reinforced short beams

Cong-Luyen Nguyen[1,*], Ngoc Han Nguyen[1], Duc Nhan Hoang[1], Quyen Cao Minh[2]

[1]Faculty of Civil Engineering, The University of Danang - University of Science and Technology, Danang, Vietnam

[2]Advanced Materials and Intelligent Systems for Infrastructure and High-Speed Rail (AMIS-HSR) Research Group, University of Transport Technology, Hanoi, Vietnam

Article info
Type of article:
Original research paper

DOI:
https://doi.org/10.58845/jstt.utt.2026.en.6.5.214-233

***Corresponding author:**
Email address:
ncluyen@dut.udn.vn

Received: 31/12/2025
Received in Revised Form: 21/10/2026
Accepted: 01/11/2026

Abstract: This study presents a numerical analysis of the shear behaviour of steel-reinforced beams made of Engineered Cementitious Composites (ECC) material. The numerical model was developed and validated using the shear performance data of three reinforced concrete (RC) short beams and one reinforced ECC (R/ECC) short beam reported in the literature. Following the validation, a parametric study was conducted to examine and evaluate the effects of ECC material properties. First, the material used in beams was changed from concrete to ECC with an equivalent nominal compressive strength, and then, by altering the ECC compressive strength, tensile strength, and tensile strain, the effects of these parameters were systematically evaluated. The results showed that replacing conventional concrete with ECC significantly enhanced the ultimate shear capacity, with shear load gains of up to 60% over the RC counterparts. By altering the ECC compressive strength, tensile strength, and tensile strain values, the subsequent parametric study revealed that the ECC tensile strength (f_t) was the dominant material parameter, leading to substantial increases in the ultimate shear load (up to 112% when f_t was increased from 1.37 MPa to 5.37 MPa). Meanwhile, the tensile strain capacity played a crucial role in enhancing the overall structural ductility and energy absorption of the R/ECC short beams. The study also found that the ECC compressive strength (f'_{cr}) had a marginal effect on the shear performance of R/ECC short beams.

Keywords: Engineered Cementitious Composites (ECC), R/ECC short beams, shear behaviour, numerical modelling, parametric study.

1. Introduction

Shear failure in reinforced concrete (RC) structures is an event that designers strive to avoid, as it is sudden, brittle, and typically offers little warning, posing significant risks to the safety of structures and human lives. Thus, structures need to be provided with sufficient shear reinforcement to avoid this unexpected failure. However, the presence of dense shear reinforcement, especially at the beam-to-column joint, leads to rebar congestion that causes construction delays and requires complex technical solutions. Materials that possess better shear performance in comparison to normal concrete are always of great importance.

For this purpose, Engineered Cementitious Composites (ECC) appears to be an appropriate candidate as it exhibits superior tensile strain capacity and features strain-hardening behavior with the formation of multiple fine cracks [1]. When combined with steel reinforcement, ECC enhances crack control, ductility, and post-cracking shear resistance, while mitigating stress concentration and improving energy absorption capacity [2-5]. Moreover, ECC characterises outperformed shear-resistant behaviour resulting from its excellent tensile strain capacity, with several times higher than that of normal concrete [6-9]. This makes ECC a promising material for the construction engineering of shear-critical structures.

A number of studies have been dedicated in order to getting insight into the shear behaviour of these structural elements [10-16]. For instance, Kanda et al. [10] employed ECC to study the shear behaviour and seismic response of coupling beams connecting shear walls. It was found from this study that the coupling beam constructed using ECC exhibited no bond splitting or shear failure. Zhang et al. [11] employed Polypropylene Fiber Reinforced Engineered Cementitious Composite (PP-ECC) to replace normal concrete to study the structural behaviour of the beam-column joint. They revealed that PP-ECC performs well in enhancing shear capacity, which could reduce the amount of transverse reinforcement required. Other scholars [12] retrofitted beam-to-column joints using ECC jackets. It has been found that ECC jackets effectively confined the joint core, mitigated localized damage through dense microcracking, and promoted a desirable flexural failure mode in the beam. This method significantly enhanced joint strength, stiffness retention, energy absorption, deformation capacity, and collapse drift, confirming its effectiveness and reliability for retrofitting exterior beam–column joints. Yang et al. [13] found the effectiveness of ECC in altering normal concrete for the cover panels of composite steel plate shear walls, by providing efficient constraint of the steel plate as well as mitigating the damage of the panels.

Short beams are usually characterized by a low shear span-to-depth ratio (normally smaller than 2.5), leading to a strut-and-tie load transfer mechanism or arch action, rather than a beam action mechanism dominated as in slender beams [17]. Thanks to this mechanism, short beams demonstrate high shear strength and stiffness, enabling them to transfer heavy loads efficiently over short spans. However, in reinforced concrete (RC) short beams, brittle shear failure often occurs prematurely, characterized by steep diagonal cracking with limited ductility, which can significantly affect the safety and serviceability of structures. It is therefore rational to introduce ECC in the short beam as a potential alternative to normal concrete due to its above-mentioned advanced performance under shear. Nevertheless, limited studies have been found in the literature that investigated the shear performance of reinforced ECC (R/ECC) short beams. Alyousif et al. [18] conducted experimental programs consisting of two comparable groups: six beams constructed with ECC and six beams made with normal concrete. Two different parameters were investigated, including three different shear span-to-depth ratios and two different amounts of longitudinal reinforcement. The experimental findings indicate that R/ECC beams exhibit superior shear performance compared to corresponding RC beams. In particular, the R/ECC specimens demonstrated notably higher load–carrying capacity, stiffness, ductility, and energy absorption. It has also been found in this study that the shear span-to-depth ratio plays a key role in the shear performance of the beams. However, the effect of ECC material, including its compressive strength, tensile strength, and strain, on the shear has not been adequately addressed [18].

In terms of numerical simulation of R/ECC short beams, there are very few studies conducted. It appears that only the study by Hamsavathi et al.

[19] examines the effects of the shear span-to-depth (a/d) ratio and shear reinforcement ratio on shear load transfer mechanisms of R/ECC short beams. From the authors' perspective, after digging into the literature, there is still a lack of in-depth analysis on the shear behaviour of R/ECC short beams with regard to the influence of ECC material on the internal stress distribution and shear behaviour of the beams. Indeed, the effects of each parameter of ECC material properties, such as compressive strength, tensile strength, and strain, on shear behaviour, including the load-displacement relationship, stress distribution, and failure mode, have yet to be investigated. Therefore, this study, in an attempt to address this gap, has conducted a numerical investigation using the Finite Element Method (FEM) to examine the shear behavior of R/ECC short beams. The findings of this study provide a deeper understanding of their structural response and establish a scientific basis for design and strengthening applications in practical engineering.

2. Development of numerical model

2.1. Specimen modelling

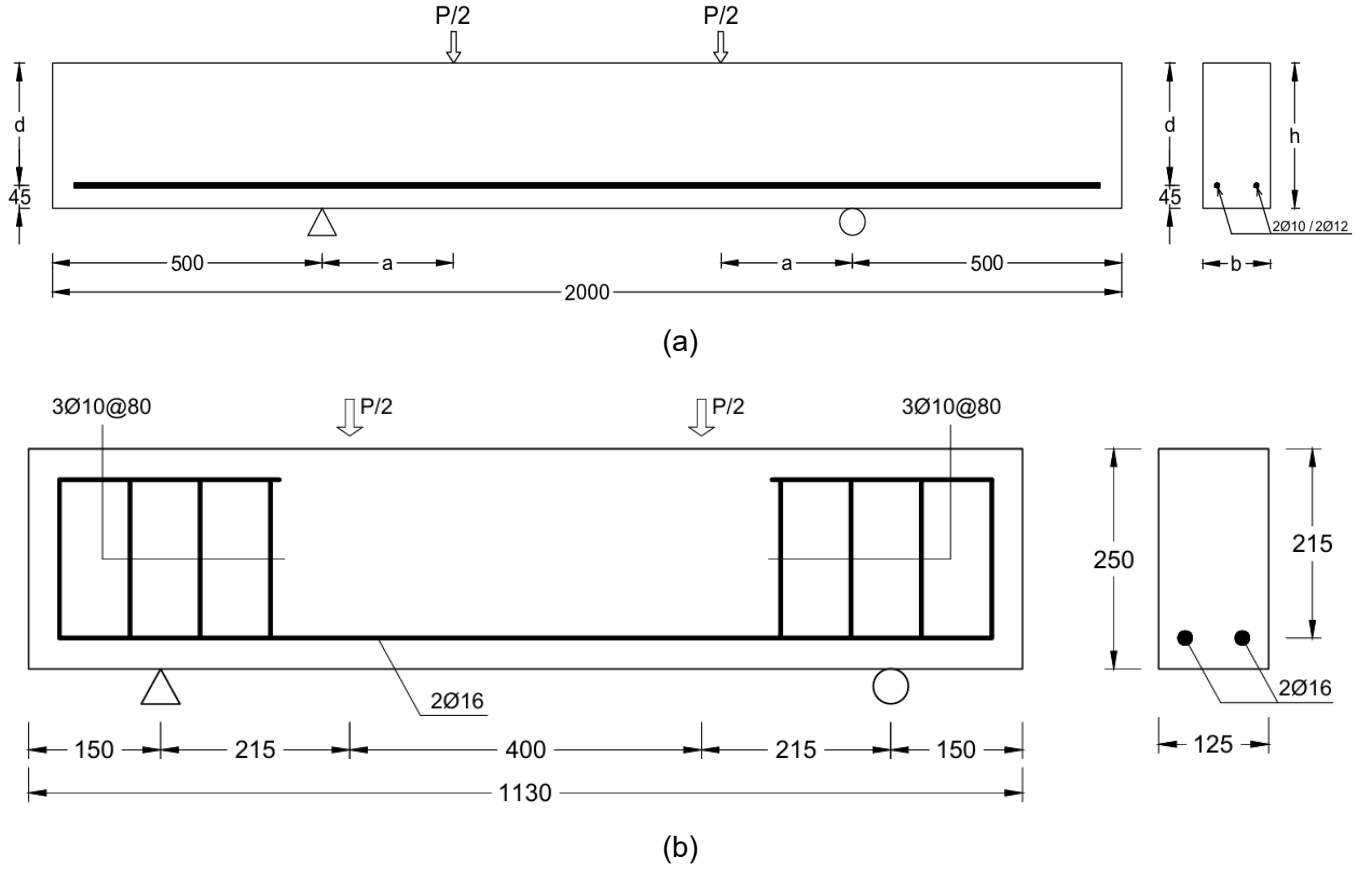


Fig. 1. Geometry and reinforcing details of the beams employed for FE modelling development: (a) RC short beams [20]; (b) R/ECC short beams [18]

Table 1. Details of the simulated beams

Source	Beam ID	b (mm)	h (mm)	a/d	Rebar	Stirrup	μ (%)	f'c* (MPa)
Ref. [20]	1.1C260-0.4	140	260	1.1	2ϕ10	-	0.4	40
	1.1C260-0.6	140	260	1.1	2ϕ12	-	0.6	40
	1.1C360-0.5	140	360	1.1	2ϕ12	-	0.5	40
Ref. [18]	ECC-1A	125	250	1.0	2ϕ16	ϕ10a80	1.29	49.1

*f'c is the compressive strength of concrete/ECC

In this study, the test program conducted by Abed et al. [20] was utilized to extract data for the development of the numerical model. Three RC short beams were selected for developing and validating the numerical model, as shown in Table 1. To further verify the reliability of the adopted numerical approach, specifically for ECC, an additional validation was performed using the experimental data of a reinforced ECC (R/ECC) short beam (labeled as ECC-1A) tested by Alyousif et al. [18]. Beam geometry and reinforcement arrangements of beams tested by Abed et al. [20] and Alyousif et al. [18] are respectively shown in Fig. 1(a) and Fig. 1(b). The details of simulated R/ECC short beams are also shown in Table 1.

2.2. Constitutive models, element types and contact properties, and boundary conditions

2.2.1. Concrete

A solid element (C3D8R) is used to simulate the concrete part. As per a recommendation shown in [20], values of the CDP (Concrete Damage Plasticity) model are shown in Table 2. The standard concrete cubes were tested and obtained an average compressive strength of 50 MPa. Therefore, the cylinder compressive strength of concrete was determined to be 40 MPa, as per Equation (1):

$$f_c^{'\,cylinder} = 0.8 f_c^{'\,cube} \quad (1)$$

where $f_c^{'\,cylinder}$ and $f_c^{'\,cube}$ are the compressive strengths of concrete of standard cylinder specimens with a diameter of 100 mm and height of 200 mm, and standard cube specimens of 150 mm in size, respectively.

The stress–strain relationship of Carreira and Chu [21] was adopted to define the stress-strain behaviour of concrete. The compressive and tensile stress-strain curves are shown in Fig. 2. The compressive behavior of concrete was assumed to be linear elastic up to compressive stress equal to $0.4f'_c$. Beyond that point, the plastic behaviour of concrete was defined using Equations (2) and (3) as follows:

$$\sigma_c = \frac{f'_c\,\gamma(\varepsilon_c/\varepsilon'_c)}{\gamma - 1 + (\varepsilon_c/\varepsilon'_c)^{\gamma}} \quad (2)$$

where: σ_c is the compressive stress in concrete, ε_c is the compressive strain in concrete, f'_c is the compressive strength of the concrete, and ε'_c is the strain when the concrete reaches compressive strength f'_c.

The γ value is calculated as follows:

$$\gamma = \left(\frac{f'_c}{32.4}\right)^3 + 1.55 \quad (3)$$

Tensile strength of concrete (f'_t) is taken as around $0.1f'_c$. The relationship between tensile stress and strain of concrete is given in Fig. 3 and is considered linear until the concrete reaches its tensile strength. After passing this stage, the tensile stress is calculated as in Equation (4):

$$\sigma_t = f_t e^{-\left(\frac{\varepsilon-\varepsilon_{cr}}{0.00035}\right)^{0.85}} \quad (4)$$

The elastic modulus of concrete is approximately calculated as in Equation (5), according to ACI 318-19:

$$E_c = 4700\sqrt{f'_c} \quad (5)$$

Table 3 presents the material parameters defining the constitutive model for the concrete used in the numerical simulations.

2.2.2. Reinforcement

The steel bars are simulated using two-node truss elements (T3D2). A bilinear curve is used for the constitutive model of reinforcement, as shown in Fig. 3. According to [20], the parameter values for the constitutive model of rebar are also shown in Table 4.

2.2.3. ECC

Similar to concrete, a solid element with reduced integration (C3D8R) is used to simulate ECC material. The stress-strain models which were reported in [22] are used for the behaviour of ECC under compression and tension, as shown in Figs. 4(a)-(b). ECC compressive stress-strain relationship is expressed as in Equation (6):

$$\sigma_c = \begin{cases} E_0\varepsilon & (0 < \varepsilon < \varepsilon_{0.4}) \\ E_0\varepsilon(1-\alpha) & (\varepsilon_{0.4} < \varepsilon < \varepsilon_0) \end{cases} \quad (6)$$

where E_0 is the elastic modulus, $\varepsilon_{0.4}$ is the strain at $0.4f'_{cr}$, ε_0 is the strain at f'_{cr}, α is the reduction coefficient of E_0 when it reaches $0.4f'_{cr}$, and α is determined as follows:

$$\alpha = a\frac{\varepsilon E_0}{f'_{cr}} - b \quad (7)$$

where coefficients a and b are 0.46 and 0.33 [22], respectively.

The ECC compressive stress-strain relationship at the post-peak stage is expressed as follows:

$$\sigma = \begin{cases} m(\varepsilon - \varepsilon_0) + f'_{cr} & (\varepsilon_0 < \varepsilon < \varepsilon_l) \\ n(\varepsilon - \varepsilon_l) + \sigma_l & (\varepsilon_l < \varepsilon < \varepsilon_{max}) \end{cases} \quad (8)$$

where the slopes of the quadratic line m and n are taken as -14190.01 and -389.60, respectively. ε_l is taken as $1{,}5\varepsilon_0$.

Table 2. The CDP parameters

Dilation Angle	Eccentricity	fb0/fc0	K	Viscosity Parameter
30	0.1	1.16	0.667	1E-6

Table 3. Parameters of concrete constitutive model adopted for FE modelling

Material	$\sigma_{0.4}$ (MPa)	$\varepsilon_{0.4}$ (%)	f'_c (MPa)	ε'_c (%)	ε_{cu} (%)	f'_t (MPa)	ε_{cr} (%)	ε_{ft} (%)
Concrete	16.0	0.0538	40.0	0.27	8.0	3.51	0.012	0.28

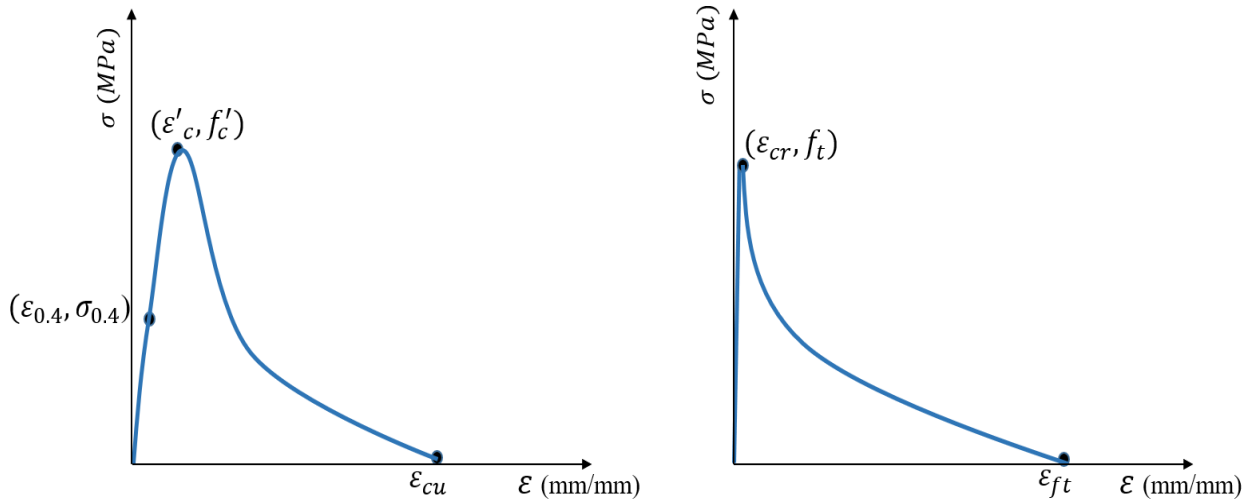


Fig. 2. Stress-strain curve in compression (left) and tension (right) of concrete

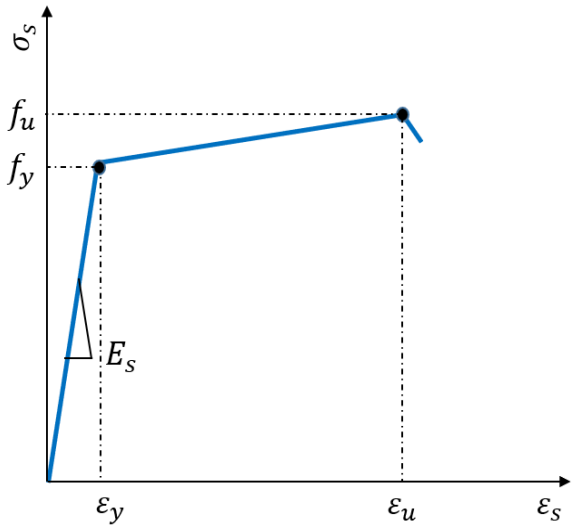
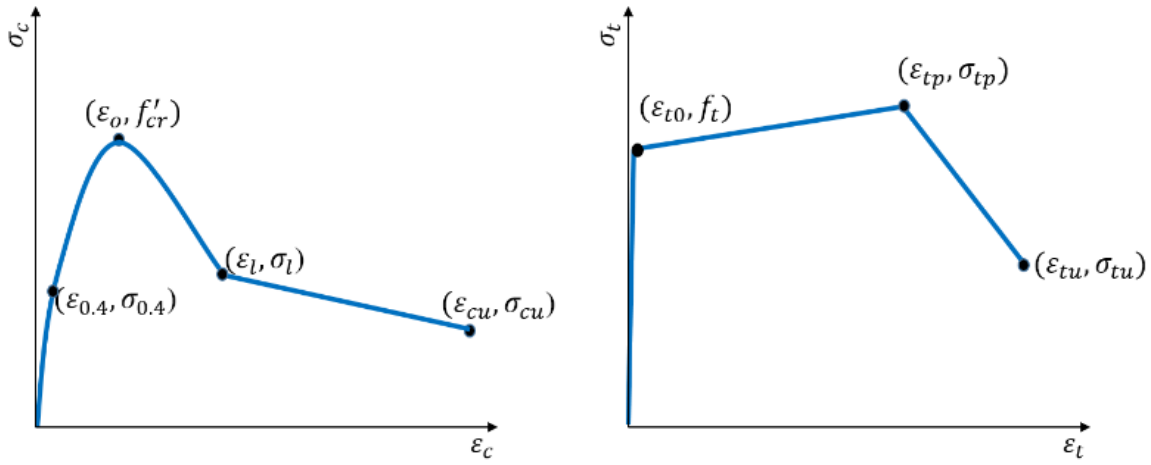


Fig. 3. Bilinear stress-strain curve of reinforcement



(a) (b)

Fig. 4. Stress-strain curve of ECC: (a) in compression; (b) in tension

Table 4. Parameters of reinforcement constitutive model

Source	Material	d_b (mm)	E_s (GPa)	ε_y (%)	f_y (MPa)	ε_u(%)	f_u (MPa)
Ref [20]	Rebar	10	200	0.21	460	12.6	690
		12	200	0.21	460	12.6	690
Ref [18]	Rebar	16	205	0.25	520	10.2	625
	Stirrup	10	198	0.22	428	9.3	535

Table 5. Parameters of ECC constitutive model adopted for FE modelling

Material	E_0 (MPa)	$\sigma_{0.4}$ (MPa)	$\varepsilon_{0.4}$ (%)	f'_{cr} (MPa)	ε_o(%)	σ_l (MPa)	ε_l (%)	σ_{cu} (MPa)	ε_{cu} (%)
ECC	18000	19.64	0.109	49.1	0.51	30.13	0.968	16.46	6.23

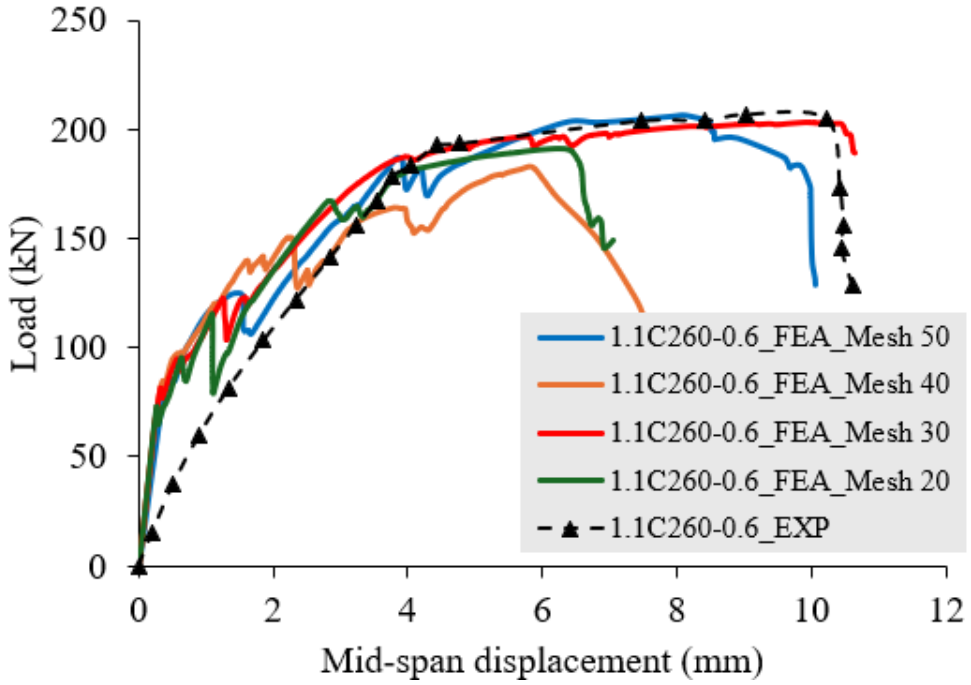


Fig. 5. Mesh sensitivity analysis

The tensile stress–strain behavior of ECC is represented by a trilinear relationship, as illustrated in Fig. 4. This simplified model is convenient for implementation in numerical simulations and has proved to be efficient in previous studies [23-25]. The tensile constitutive response is defined by

Equation (9), which can be written as follows:

$$\sigma_t = \begin{cases} E_0\varepsilon & 0 \le \varepsilon \le \varepsilon_{t0} \\ \sigma_{t0} + (\sigma_{tp} - \sigma_{t0})\left(\frac{\varepsilon-\varepsilon_{t0}}{\varepsilon_{tp}-\varepsilon_{t0}}\right) & \varepsilon_{t0} \le \varepsilon \le \varepsilon_{tp} \\ \sigma_{tp}\left(1-\frac{\varepsilon-\varepsilon_{t0}}{\varepsilon_{tp}-\varepsilon_{t0}}\right) & \varepsilon_{tp} \le \varepsilon \le \varepsilon_{tu} \\ 0 & \varepsilon_{tu} < \varepsilon \end{cases} \quad (9)$$

where: σ_{t0} and ε_{t0} are the first crack stress and corresponding strain, σ_{tp} is the tensile stress and ε_{tp} is the corresponding strain, ε_{tu} is the failure strain. The parameters of the ECC constitutive model adopted for FE modelling are shown in Table 5.

2.2.4. Contact properties and boundary conditions

The support and load plates were tied to the beam using a tie constraint available in Abaqus. For the contact between concrete/ECC and reinforcement, the embedded region option was used. Boundary conditions were applied to two support plates of the beam, in which one acted as the pinned support and the other acted as the roller support. For the pinned support, all three directions were fixed to move for the nodes situated at the bottom middle line of the support plate. Whereas, the corresponding nodes were fixed in only two directions and free to move in the longitudinal beam axis for the roller support.

The beam volume was discretized using brick elements with reduced integration, with a nominal element size of 30 mm for the concrete/ECC after a sensitivity analysis was conducted, which is shown in Fig. 5. As can be seen in Fig. 5, the numerical results using the mesh size of 30 mm for brick elements show the most accuracy in terms of both load capacity and displacement at failure. In addition, the selection of a 30 mm mesh size ensures the modelling accuracy and computational time efficiency. Fig. 6 illustrates the typical geometry, meshing strategy, boundary conditions, and loading setup adopted for the numerical analysis. The load was applied via displacement-controlled loading at two loading plates.

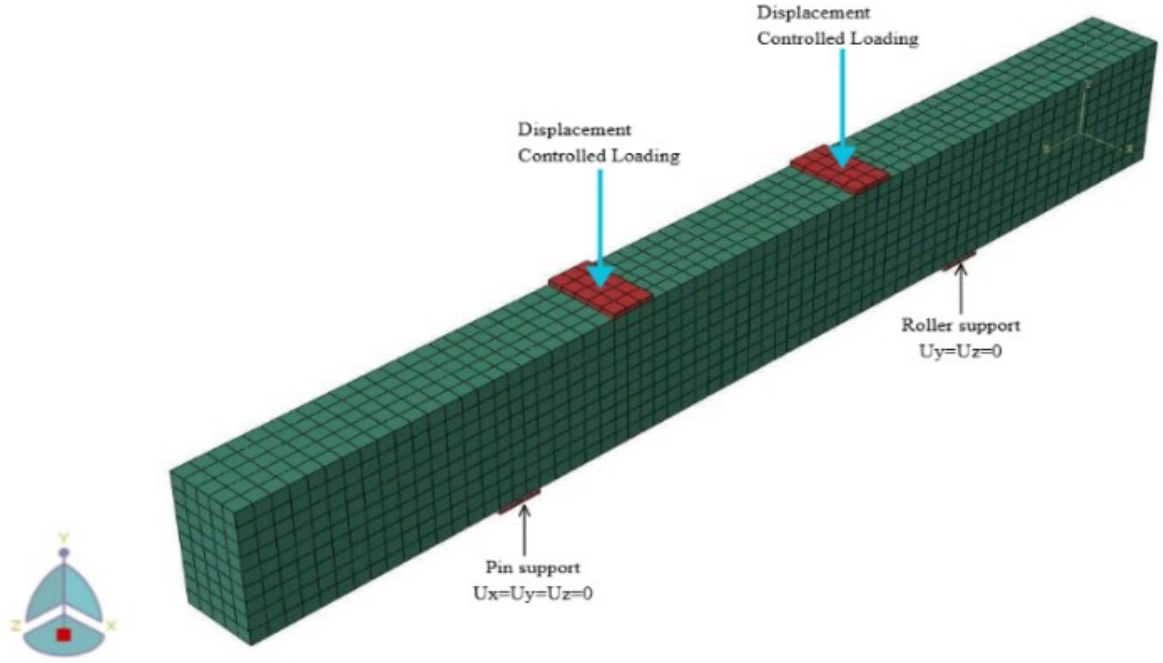


Fig. 6. A typical FE mesh (with 30 mm nominal element size) used for the modelling of beams

3. Validation of numerical model

3.1. Validation using RC short beams

The validation results, comparing the Finite Element Analysis (FEA) predictions with the experimental data (EXP) for all three RC short beams (1.1C260-0.4, 1.1C260-0.6, and 1.1C360-0.5), demonstrate a satisfactory agreement in terms of the load–midspan displacement curves, as shown in Figs. 7(a)-(c). The results indicate that, despite being slightly higher in terms of initial

bending stiffness, the FE model results align well with the experimental data regarding the yielding point and maximum load-carrying capacity.

Fig. 8(a) shows the crack distribution comparison between the experiment and the FEA for the three RC short beams. The numerical model demonstrates good agreement in capturing the shear failure mechanism. Both experimental and numerical results consistently reveal a shear-dominated failure mode, characterized by the propagation of a single, critical diagonal shear crack extending from the support to the loading point, which is a typical failure in short beams. Specifically, the FE model accurately predicts the location and orientation of these critical shear cracks. For all three beams, the simulation results effectively capture the high stress concentration consistent with a shear-compression failure near the loading point. This strong alignment between the model's damage prediction and the physical experimental observation provides strong evidence validating the stability and reliability of the developed numerical models.

Table 6 summarizes the comparison between the numerical finite element (FE) results and the experimental data for the three RC short beams. The FE model demonstrates good accuracy in predicting the load-carrying capacities. The deviation for the ultimate load across all three beams is consistently very low, ranging from just 0.4 % to 1.7 %. Similarly, the deviation for the yield load is also small, ranging from 0.2% to 6.4%. This confirms that the developed numerical model is capable of capturing the stiffness and strength mechanisms of the RC short beams. The deviation for ultimate displacement is also relatively low, ranging from 2.9% to 4.3%. The maximum deviation in yield displacement is for beam 1.1C360-0.5, which is shown at 33.7%. That is the most sensitive parameter in the model, possibly due to minor differences in defining the yield point in the experimental data versus the numerical simulation.

Figs. 9(a)-(c) demonstrate a reasonable and close agreement between the load-strain curves in rebar derived from the FE model and the EXP results for all three RC short beam specimens. This high degree of correlation serves as a strong validation for the numerical model. The FEA curves closely match the EXP curves during the initial elastic loading stage, despite a slightly higher strain. Then the FEA results accurately capture the onset of steel yielding in all three short beams. After yielding of steel, all three beams reached the strain hardening stage and failed at a certain mid-span displacement. From Figs. 7(a)-(c) to Figs. 9(a)-(c), it is said that the numerical model has been validated with the experimental results in three typical RC short beams, including the load-displacement relationship, crack distribution, and load-strain relationship of rebar, demonstrating it as a reliable tool for subsequent parametric study investigation on the effect of different parameters on the shear behaviour of short beams.

3.2. Validation using R/ECC short beams

Figs. 7(d) and 8(b) compare the numerical predictions with the experimental results [18] for the R/ECC short beam. As illustrated in Fig. 7(d), the simulated load-displacement curve captures the initial stiffness, peak shear capacity, and post-peak softening behavior with a high degree of accuracy. Fig. 8(b) presents the numerical failure mode of the simulated R/ECC short beam. It can be observed that the R/ECC short beam developed a broader and more distributed diagonal damage pattern rather than a single, highly localized major diagonal crack. This distributed damage response in the macroscopic model conceptually reflects the high tensile strain capacity and the strain-hardening properties of the ECC material. Moreover, the numerically simulated R/ECC short beam also exhibited localized crushing at the loading point and supports due to stress concentration, which generally aligns with experimental observations. The deviations in yield and ultimate loads between FE and test results

shown in Table 6 are only around 5%. Overall, the numerical model demonstrates a reasonable capability in capturing the load-displacement curve, shear carrying capacity, and primary shear failure mechanisms of R/ECC short beams, providing satisfactory support for the reliability of the developed numerical approach within the investigated scope.

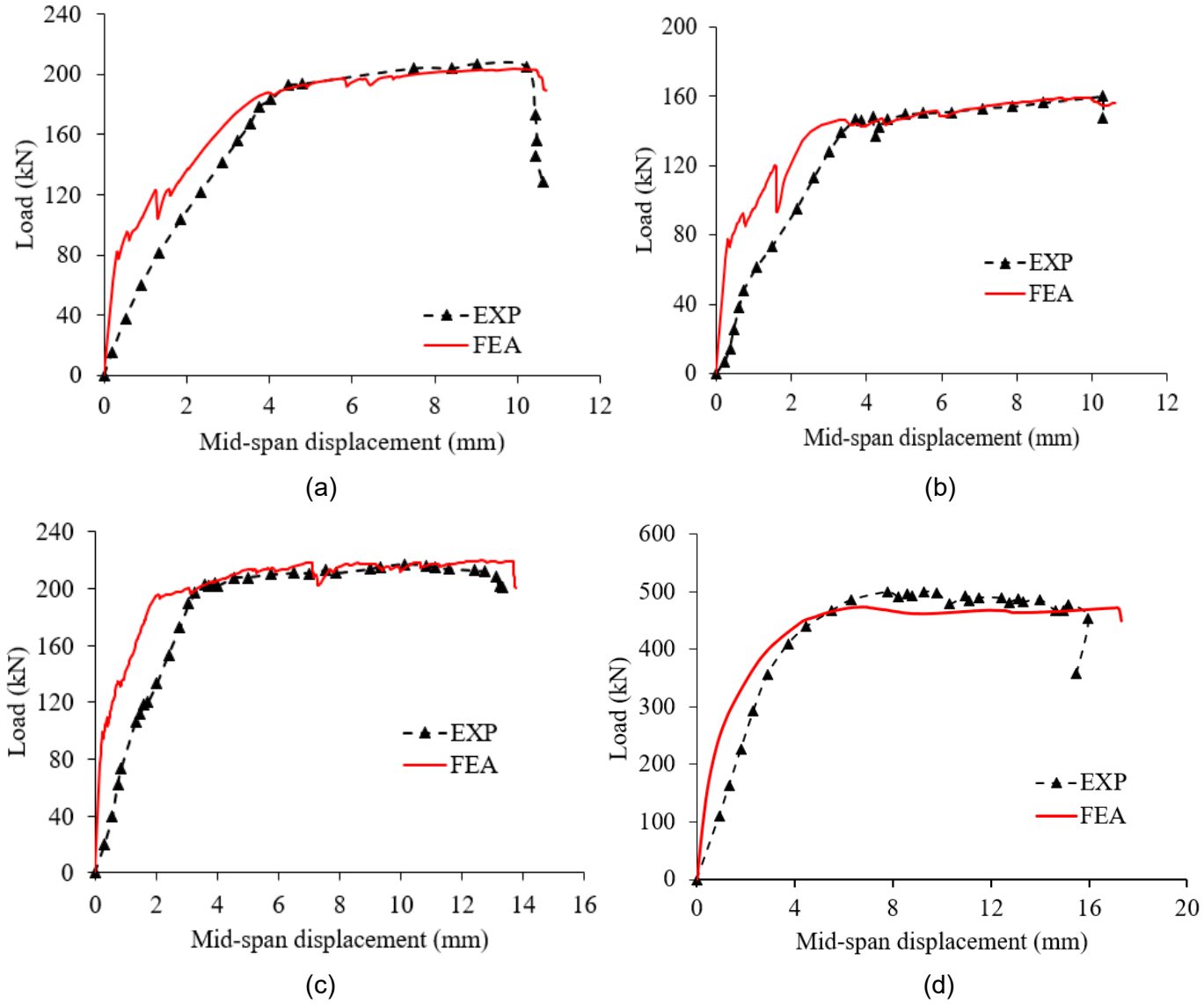
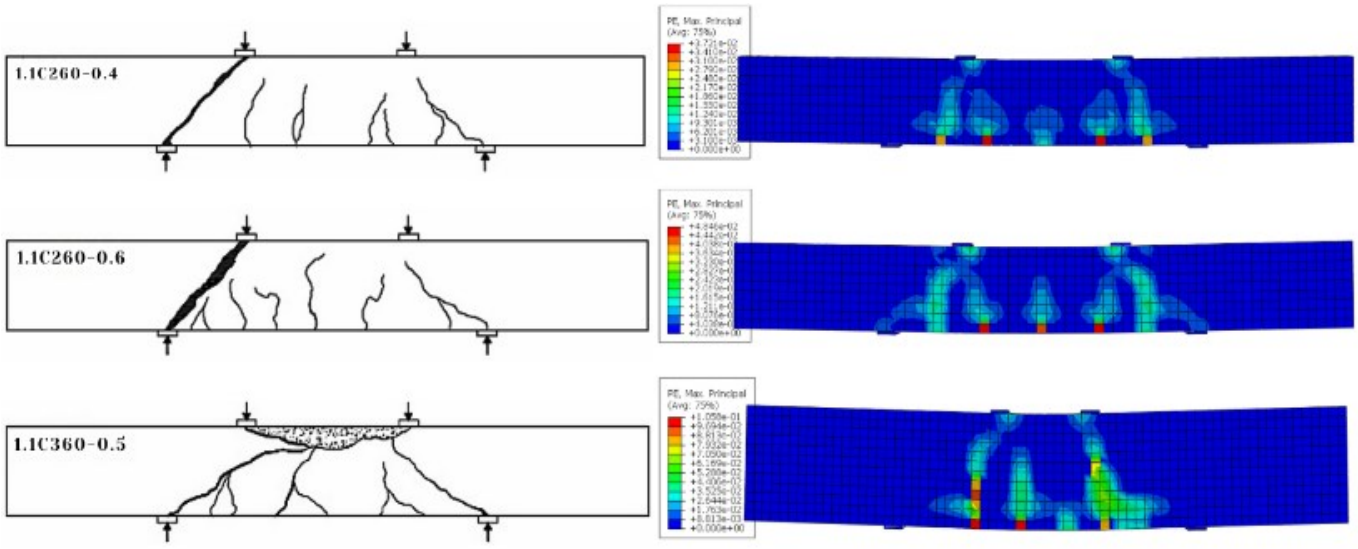


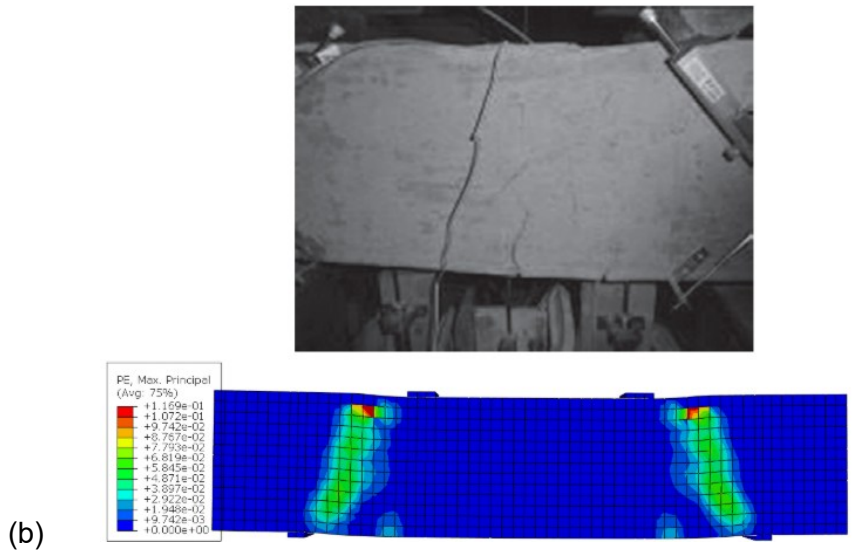
Fig. 7. Load - displacement relationship of short beams compared between FEA and experimental results of [18], [20]: (a) 1.1C260-0.6 beam; (b) 1.1C260-0.4 beam; (c) 1.1C360-0.5 beam; (d) ECC-1A beam

Table 6. Comparison of FE models and experimental results [18, 20]

Beam	Yield load (kN)		Dev. (%)	Yield disp. (mm)		Dev. (%)	Ultimate load (kN)		Dev. (%)	Ultimate disp. (mm)		Dev. (%)
	EXP	FE		EXP	FE		EXP	FE		EXP	FE	
1.1C260-0.4	143.5	139.8	2.5	3.7	2.8	24.9	160.0	159.4	0.4	10.3	9.9	4.3
1.1C260-0.6	186.4	187.8	0.2	4.1	4.0	2.9	203.3	201.1	1.1	10.1	10.5	3.5
1.1C360-0.5	203.1	190.0	6.4	2.1	3.2	33.7	211.9	208.3	1.7	12.8	13.1	2.9
ECC-1A	466.67	455.95	2.3	5.5	4.7	17.0	499.2	473.5	5.5	7.6	6.9	10.1

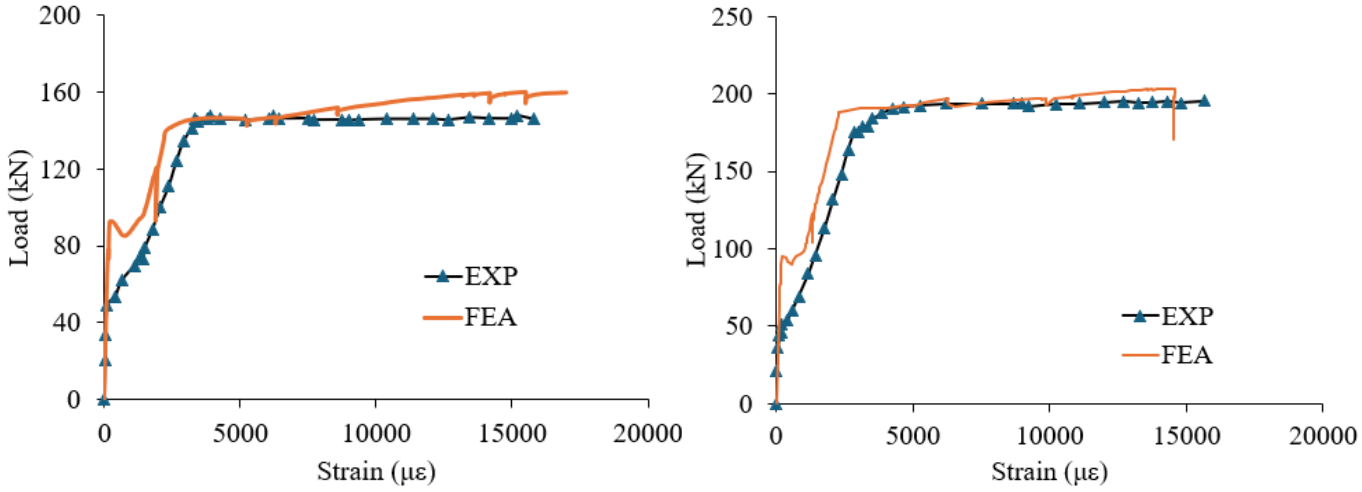


(a)



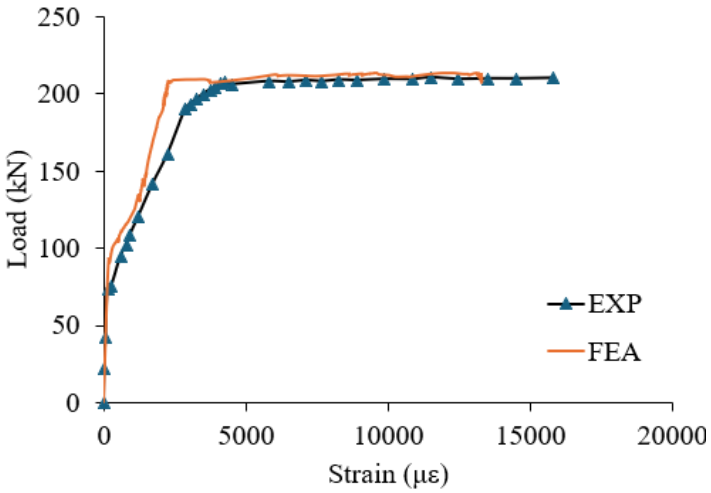
(b)

Fig. 8. Failure modes of simulated beam specimens compared with experimental results [18], [20]: (a) RC short beams; (b) R/ECC short beam (ECC-1A)



(a) (b)

Fig. 9. Load - strain relationship of rebar of RC short beams compared between FEA and test results [20]: (a) 1.1C260-0.4 beam; (b) 1.1C260-0.6 beam; (c) 1.1C360-0.5 beam



(c)

Fig. 9. (continued)

4. Effect of ECC material on shear behaviour of R/ECC short beams

4.1. Effect of ECC material

This section presents the primary comparative study of the numerical investigation. The main objective is to directly quantify the structural behaviour when replacing conventional concrete with ECC in short beam specimens. Three R/ECC beams were modeled using the approach established in Section 3. Basically, the beams were designed with identical geometric dimensions, reinforcement ratios (μ), and equivalent nominal material properties (the identical compressive strength between ECC and concrete). It is important to clarify that this is not a simple equal-strength material replacement. While the nominal compressive strengths are identical, ECC and conventional concrete possess fundamentally different constitutive responses, particularly regarding their elastic modulus, tensile strength, ultimate strain capacity, and cracking mechanisms. Therefore, this baseline comparison specifically aims to highlight the structural advantages derived from the unique tensile and strain-hardening properties of ECC compared to the brittle nature of conventional concrete. The modelled R/ECC short beams are labelled in the same way as presented for RC beams; however, the letter C is now replaced by the letter E to represent the ECC material. The parameters used for the three R/ECC short beams are tabulated in Table 7. Table 8 summarizes the parameters adopted for the ECC behaviour under compression, whereas Table 9 provides the corresponding parameters defining the tensile constitutive response, including the critical strain-hardening and ultimate tensile strain capacities. These material property parameters were selected based on the experimental results conducted in previous studies [22, 26, 27]. It is noted that these simulated R/ECC short beams employed material parameters of ECC 40 MPa, which are similar to those of simulated RC short beams in terms of cementitious material grade.

The numerical results discussion focuses on comparing the load-displacement response, ultimate shear capacity, shear-carrying mechanism, and failure mode between the beam specimens employing these two materials. In all three comparative pairs (1.1C260-0.4 vs 1.1E260-0.4, 1.1C260-0.6 vs 1.1E260-0.6, and 1.1C360-0.5 vs 1.1E360-0.5), the R/ECC short beams exhibited a significantly higher ultimate shear capacity than their concrete counterparts, as shown in Figs. 10(a)-(c). The load increase for the R/ECC short beams is substantial, ranging from approximately 25% to 60% depending on the specimen geometry and reinforcement ratio. The

R/ECC short beams consistently displayed superior displacement. Despite exhibiting a slightly lower initial stiffness, the R/ECC short beams maintained their significantly higher peak load in comparison to their concrete counterparts. These findings are concretely supported by the experimental program previously conducted by Alyousif et al. [18].

Table 7. Details of the simulated beams

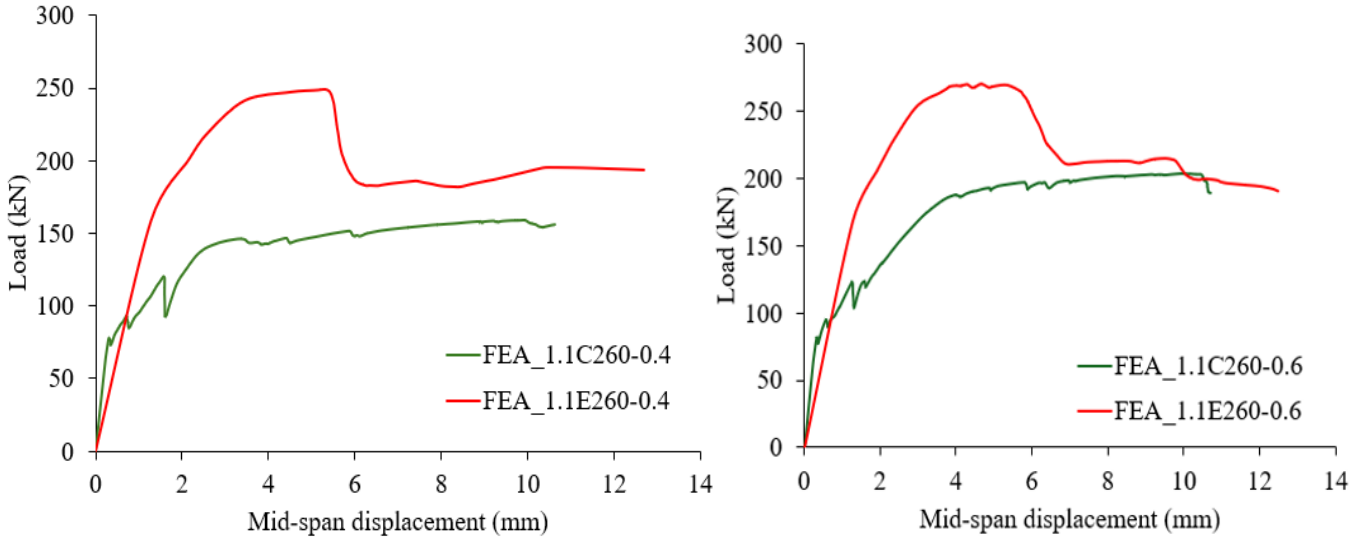
Name	b (mm)	h (mm)	a/d	Rebar	μ (%)	f'cr (MPa)
1.1E260-0.4	140	260	1.1	2ϕ10	0.4	40
1.1E260-0.6	140	260	1.1	2ϕ12	0.6	40
1.1E360-0.5	140	360	1.1	2ϕ12	0.5	40

Table 8. Parameters of ECC constitutive models in compression

Material	E_c (MPa)	$\sigma_{0.4}$ (MPa)	$\varepsilon_{0.4}$ (%)	f'_{cr} (MPa)	ε_o(%)	σ_1 (MPa)	ε_1 (%)	σ_{cu} (MPa)	ε_{cu} (%)
ECC 20MPa	10300	8.01	0.100	20.11	0.375	14.03	0.891	7.92	4.55
ECC 40MPa	15300	16.01	0.105	40.21	0.395	28.06	0.935	15.84	5.47
ECC 60MPa	20300	24.02	0.110	60.32	0.413	42.09	0.975	23.76	6.86

Table 9. Parameters of ECC constitutive models in tension

Material	f_t (MPa)	ε_{t0} (%)	σ_{tp} (MPa)	ε_{tp} (%)	σ_{tu} (MPa)	ε_{tu} (%)
ECC 20MPa	2.30	0.020	2.50	0.70	0.11	1.78
ECC 40MPa	3.37	0.022	4.06	0.80	0.21	1.88
ECC 60MPa	4.88	0.027	5.30	0.95	0.27	2.02



(a) (b)

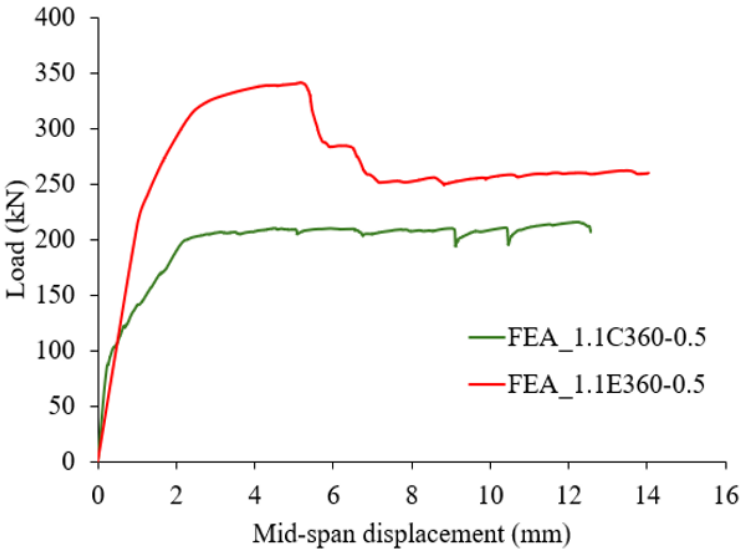
Fig. 10. Comparison of numerical results between RC and R/ECC beams: (a) 1.1C260-0.4 vs 1.1E260-0.4; (b) 1.1C260-0.6 vs 1.1E260-0.6; (c) 1.1C360-0.5 vs 1.1E360-0.5

Based on the visual comparison of maximum principal stress contours between the simulated R/ECC short beams and the RC short beam specimens (Figs. 11(a)-(c)), it can be seen that the R/ECC short beams exhibit a substantial arch action compared to RC counterparts, especially in beam 1.1E360-0.5, which correspondingly allows the R/ECC short beams to resist higher shear loads and larger displacements.

4.2. Effect of ECC grade

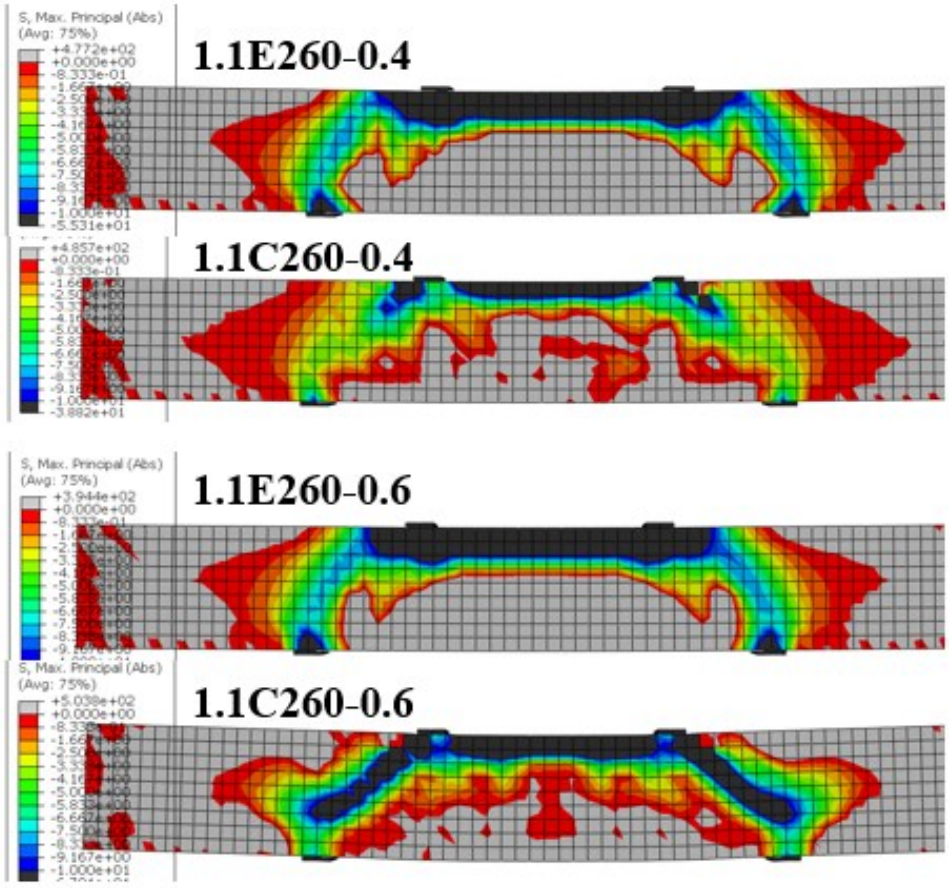
To evaluate the shear performance of R/ECC short beams under realistic material conditions, a parametric study was conducted considering comprehensive ECC grades. In practice, the

material properties of cementitious composites are interlinked; an increase in compressive strength (f'_{cr}) is typically accompanied by enhancements in elastic modulus (E_0) and tensile strength (f_t). Therefore, three distinct ECC grades were simulated, including ECC 20 MPa, ECC 40 MPa (the baseline), and ECC 60 MPa. The material parameters input for numerical analysis of each ECC grade are tabulated in Tables 8 and 9. Where the parameters were proportionally adjusted to reflect established empirical correlations for realistic mix designs.



(c)

Fig. 10. (continued)



(a)

(b)

Fig. 11. Maximum principal stress distribution in R/ECC and RC short beams: (a) 1.1C260-0.4 vs 1.1E260-0.4; (b) 1.1C260-0.6 vs 1.1E260-0.6; (c) 1.1C360-0.5 vs 1.1E360-0.5

(c)

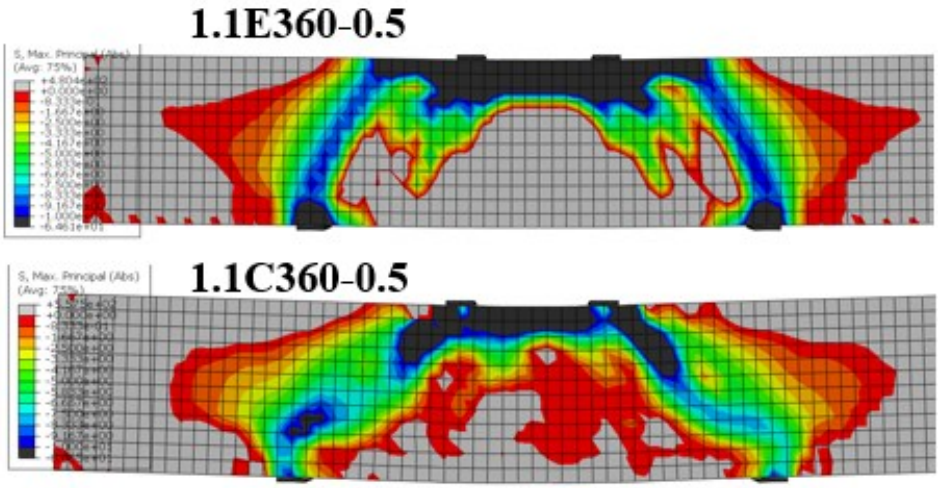


Fig. 11. (continued)

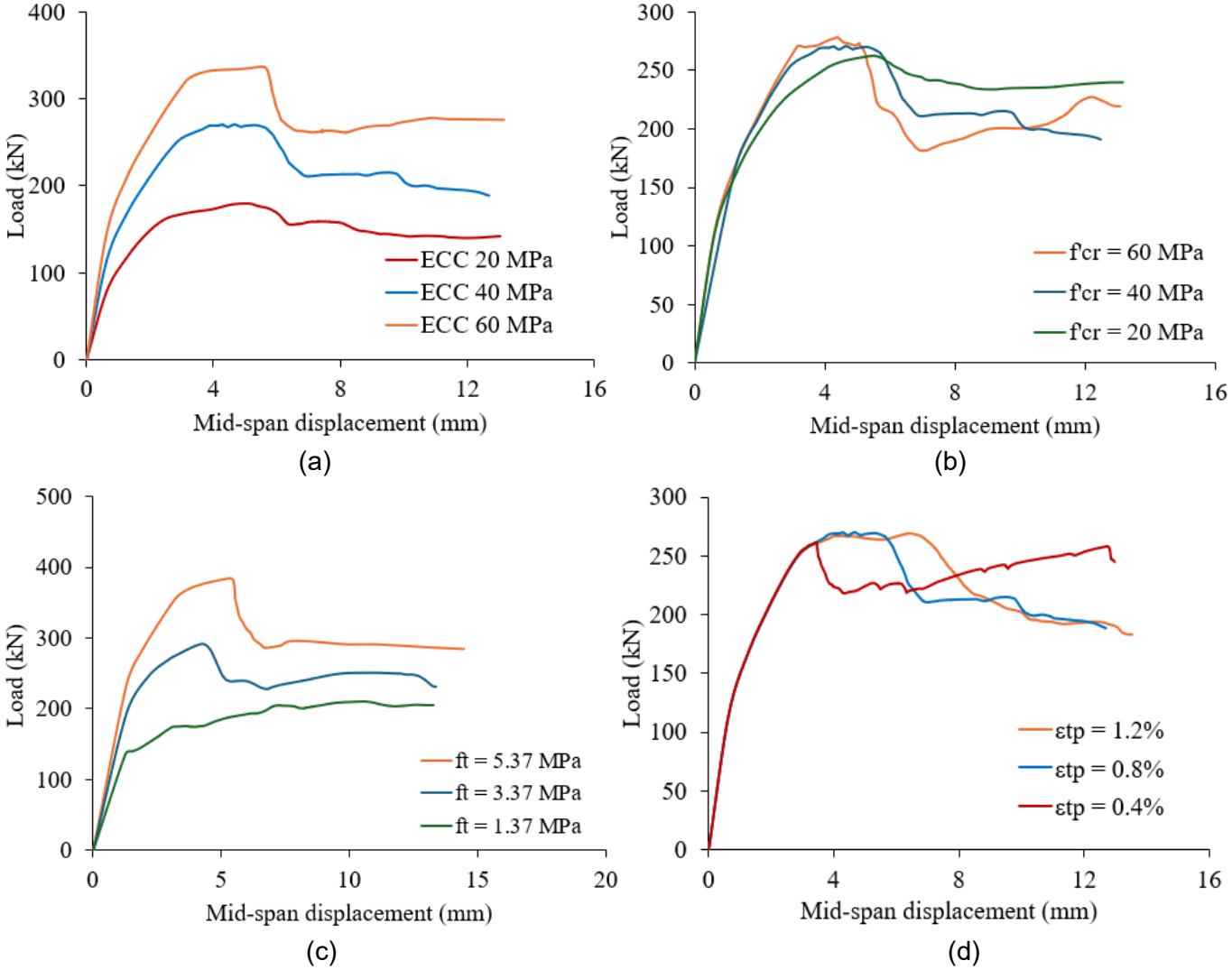


Fig. 12. Load-displacement curves of beams with different: (a) ECC grade; (b) ECC compressive strength; (c) ECC tensile strength; (d) ECC tensile strain

The load-midspan displacement curves for the three ECC grades are presented in Fig. 12(a). The results clearly demonstrate that upgrading the ECC material grade significantly enhances the overall shear performance of the R/ECC short beams. First, a distinct variation in the initial

stiffness is observed among the three curves; the ECC 60 MPa beam case exhibits the steepest elastic slope, directly reflecting the higher elastic modulus of the higher grade. Second, the ultimate shear capacity is substantially improved, jumping from approximately 180 kN for the ECC 20 MPa grade to nearly 270 kN for the ECC 40 MPa grade, and reaching approximately 340 kN for the ECC 60 MPa grade. Despite these dramatic increases in stiffness and peak load, all three beams reached their ultimate capacity at a relatively consistent mid-span displacement (4-6 mm) and exhibited a similar stable post-peak softening phase. To further systematically determine exactly which individual material parameter (f'_{cr}, f_t, or tensile strain ε_{tp}) predominantly drives these significant performance gains observed across different grades, a strictly isolated parameter investigation is subsequently presented in the following sections.

4.3. Effect of ECC compressive strength

The investigation utilized the baseline R/ECC beam model (beam 1.1E260-0.6 with f'_{cr} = 40 MPa) and introduced two additional numerical beam specimens with f'_{cr} varying from 20 MPa to 60 MPa. It is noted that in this strictly controlled numerical study, only the compressive strength parameter was varied while all other constitutive parameters, including the elastic modulus, the tensile strength, the CDP parameters, and the strain at peak compressive strength, were fixed at constant values, which is intended merely to clearly demonstrate the effect of the ECC compressive strength parameter on the shear performance of ECC short beams.

As shown in Fig. 12(b), it can be observed that peak loads of the three R/ECC short beams with various compressive strengths (20, 40, and 60 MPa) differ by only about 5 – 7%, despite the compressive strength of the ECC increasing up to 200% (from 20 to 60 MPa). All three curves exhibit nearly identical initial stiffness, as the elastic modulus was intentionally kept constant regardless of f'_{cr}. The peak loads were reached at similar displacements (about 4-6 mm), suggesting that the onset of shear-critical damage is not strongly influenced by compressive strength. To further clarify the shear-carrying mechanism in these R/ECC short beams, a Von-Mises stress contour at the failure point is plotted in Fig. 13 for the R/ECC short beam with f'_{cr} of 60 MPa. It is seen that even though the compressive strength of ECC is 60 MPa, the compressive stress developed at the compression tie is only about 25 MPa at failure, which means that the ties did not fail, and the beam failed due to the failure of the ECC diagonal strut. This explicitly explains the marginal effect of compressive strength on the shear performance of R/ECC short beams.

4.4. Effect of ECC tensile strength

The influence of the ECC tensile strength, which is a critical attribute governing cracking resistance and strain-hardening behavior, is worth conducting an investigation. To isolate this variable, the baseline ECC beam model (1.1E260-0.6), featuring a tensile strength of f_t = 3.37 MPa, was utilized as the control specimen. The parametric investigation involved simulating two additional beams in which the tensile strength was systematically varied to f_t = 1.37 MPa and 5.37 MPa. It is worth mentioning that all other ECC material parameters, including the compressive strength (f'_{cr}), elastic modulus, and especially the ultimate tensile strain, were fixed at constant values. This strict control enables the direct investigation of the relationship between tensile strength and the shear transfer mechanism of the ECC short beams, thereby quantifying the contribution of fiber bridging to the peak load capacity and post-peak behaviour.

As shown in Fig. 12(c), unlike the compressive strength case, the curves indicate that a higher f_t leads to a noticeable increase in the initial stiffness and the slope of the curve before the peak load. When f_t increases from 1.37 MPa to 5.37 MPa, the load-carrying capacity doubles from 175

kN to 372 kN, confirming that the shear resistance is highly dependent on the tensile strength of the ECC. Figs. 14(a)-(c) explain that the increase in f_t leads to the substantial buildup of arch action in R/ECC short beams, which results in the increase of shear capacity. However, it should be highlighted that these numerical results were achieved based on the simplified trilinear tensile stress-strain model of ECC. Even though this simplified tensile stress-strain model is proven to be efficient in previous studies [23-25], it might not fully represent the complex micromechanical behaviours of ECC with multiple tiny crack formation and fiber-bridging mechanisms. Therefore, more experimental as well as analytical work needs to be systematically carried out in the future to clarify this phenomenon.

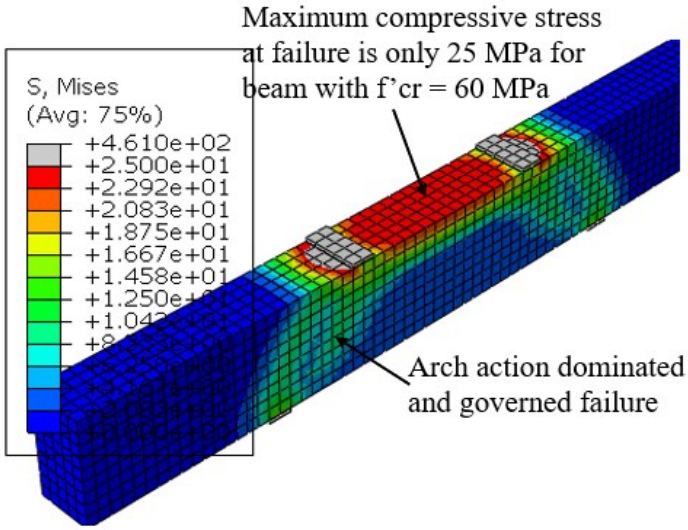


Fig. 13. Von-Mises stress contour in beam with f'_{cr} = 60 MPa

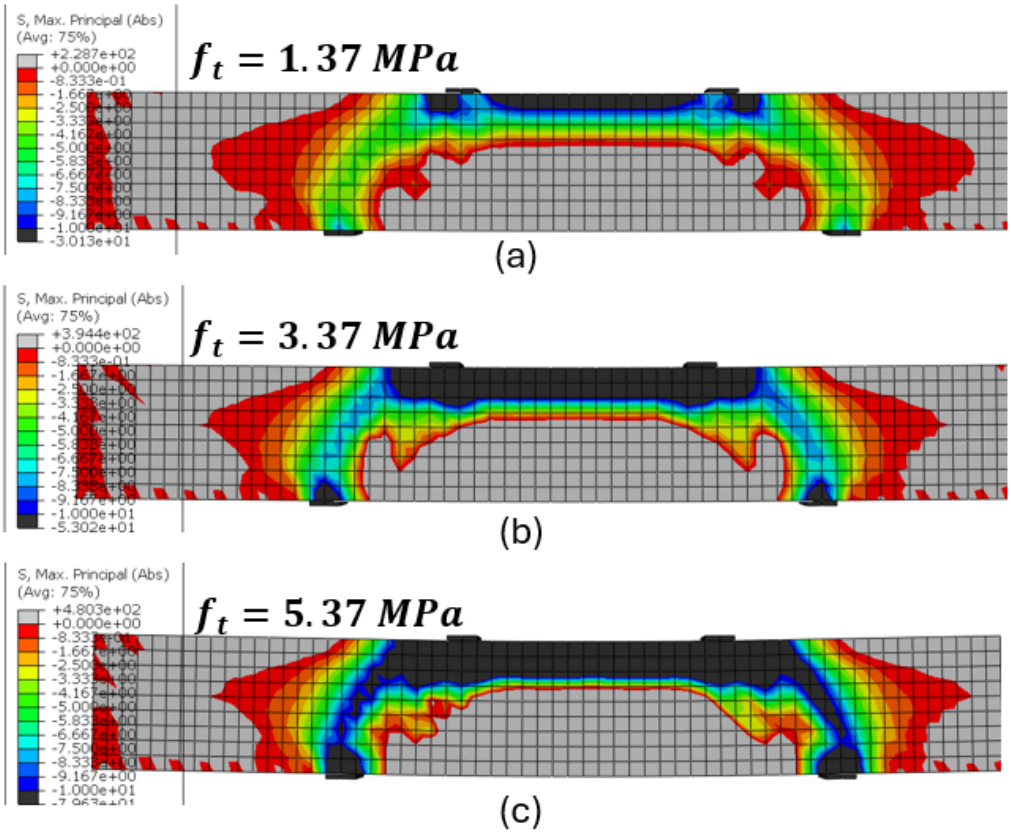


Fig. 14. Arch action built in R/ECC short beams with different f_t: (a) f_t = 1.37 MPa; (b) f_t = 3.37 MPa; (c) f_t = 5.37 MPa

To provide quantitative evidence for the enhanced structural resilience, the actual energy absorption of the simulated beams was evaluated. This energy absorption was calculated by integrating the area under the load-displacement relationship. To ensure a consistent and objective comparison across all models, the integration limit for each specimen was strictly defined as the displacement point at which the post-peak load degraded to 80% of its ultimate capacity [28]. Fig. 15 demonstrates that a higher f_t value results in a higher energy absorption, with an increase of up to 43% when increasing f_t from 1.37 MPa to 5.37 MPa.

4.5. Effect of ECC tensile strain

In order to study the influence of the tensile strain capacity (ε_{tp}) of ECC, which is a key parameter dictating the material's ductility and its ability to maintain stress transfer across a wide crack, on the shear-resistant behaviour of R/ECC short beams, three beam cases were modeled with different tensile strain capacities. The baseline ECC beam model (1.1E260-0.6), featuring an initial ε_{tp} of 0.8%, was used as the control specimen. The investigation involved simulating two additional numerical beams where the tensile strain was systematically increased to 1.2% and decreased to 0.4%. It is noted that this tensile strain range is commonly achievable for ECC, as it is well-known for excellent strain-hardening behaviour, and its tensile strain normally exceeds 2%.

The load-displacement results of these three beams are shown in Fig. 12(d). It is indicated that all three R/ECC short beams, regardless of the ε_{tp} value, achieve a nearly identical ultimate load capacity (approximately 260 kN to 270 kN) and exhibit similar initial stiffness up to the peak. The ε_{tp} = 1.2% curve shows the most stable softening, sustaining a high residual load up to 7.2 mm displacement. Conversely, the ε_{tp} = 0.4 % curve exhibits the most brittle post-peak drop and the lowest residual strength, resembling a material that loses its fiber bridging capacity prematurely. The energy absorption of beams with different tensile strain, shown in Fig. 15, demonstrates that a higher ε_{tp} allows the ECC to have a greater inelastic strain, resulting in superior ductility and better energy absorption capability for the beam.

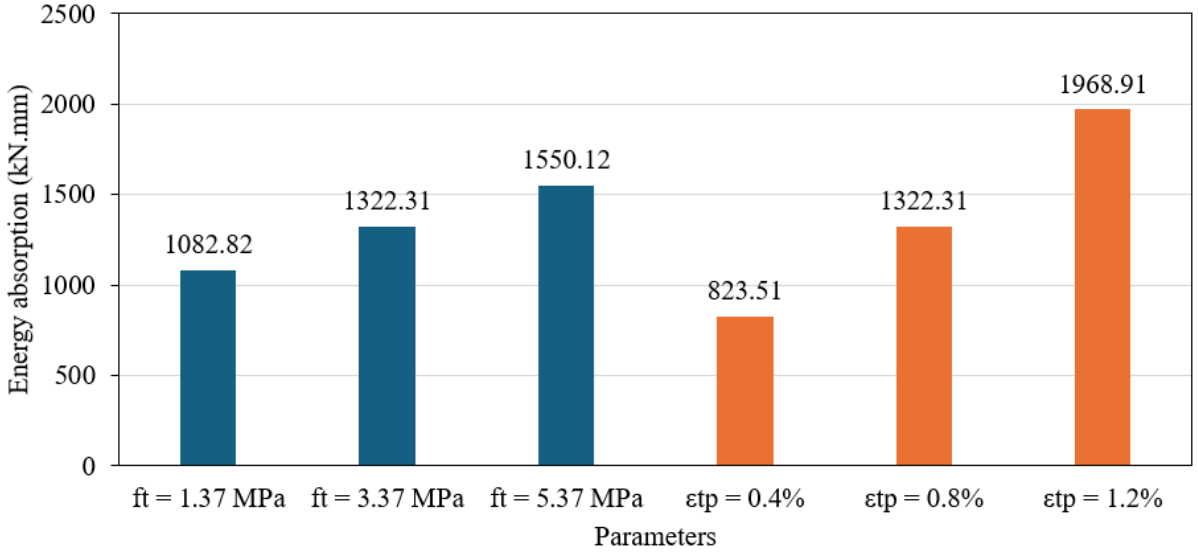


Fig. 15. Comparison of energy absorption for R/ECC short beams with varying tensile strength and tensile strain capacities

5. Conclusions

A numerical analysis of the shear behaviour of RC and R/ECC short beams was conducted in this study. The numerical model was developed using finite element method-based software named Abaqus. Nonlinearities of materials and real contacts between components were carefully considered in the study. The numerical model was

validated using the experimental data of three RC short beams and one R/ECC short beam reported in the literature. Following the validation, a parametric study was conducted to examine and evaluate the effects of ECC material on the shear behaviour of the R/ECC short beams. Several conclusions can be drawn from this study:

- The numerical model developed in this study aligned well with the experimental data of RC and R/ECC short beams, not only in terms of shear load-displacement relationship but also in terms of crack distribution and load-strain behaviour of the rebar. This demonstrates that the developed numerical model adequately captures the fundamental shear response within the investigated scope, providing a reliable basis for the subsequent parametric study.

- By replacing conventional concrete with ECC with an equivalent nominal compressive strength, the numerical results indicated that, within the simulated configuration range, ECC can notably enhance both the ultimate shear capacity and ductility. An increase of up to approximately 60% in shear capacity was observed for the simulated R/ECC short beams over their RC counterparts, thanks to the excellent strain capacity of ECC in tension and shear.

By altering the ECC grade, ECC compressive strength, tensile strength, and tensile strain values, the effects of these parameters were systematically evaluated. It has been revealed that the ECC tensile strength is the dominant material parameter, leading to substantial increases in the ultimate load (up to 112% when f_t was increased from 1.37 MPa to 5.37 MPa). This shear strength increase is accounted for by the substantial buildup of arch action in R/ECC short beams with higher tensile strength. Meanwhile, the tensile strain capacity played a crucial role in enhancing the overall structural ductility and energy absorption of the R/ECC short beams. It has also been found that the compressive strength has a marginal effect on the shear performance of R/ECC short beams due to the fact that the arch action governs the failure in these R/ECC short beams. However, it should be highlighted that these numerical results were achieved based on the simplified trilinear tensile stress–strain model of ECC and an idealized one-variable-at-a-time parametric design, which might not fully represent the complex micromechanical behaviours of ECC, including the formation of multiple microcracks and fibre-bridging mechanisms. Therefore, more experimental and analytical work needs to be systematically carried out in the future to clarify this phenomenon.

Declaration of Generative AI

During the preparation of this work, the authors used ChatGPT (OpenAI) in order to improve the readability and language of the manuscript. After using this tool, the author(s) reviewed and edited the content as needed and take full responsibility for the content of the published article.

References

[1] V.C. Li. (2003). On engineered cementitious composites (ECC) a review of the material and its applications. *Journal of Advanced Concrete Technology*, 1(3), 215-230. DOI: https://doi.org/10.3151/jact.1.215

[2] J. Yang, L. Jiang, H. Guo, G. Yao. (2023). Stress mechanism and energy dissipation performance optimization of prefabricated ECC/RC combined shear walls under low cyclic loading. *Buildings*, 13(3), 772. DOI: https://doi.org/10.3390/buildings13030772

[3] J. Tian, X. Wu, Y. Zuo, J. Yuan, W.-W. Wang. (2024). Interface behaviors between smart-functional ECC and steel rebar under coupling effect of sustained load and chloride ion erosion: Corrosion resistance, mechanical and self-sensing properties. *Construction and Building Materials*, 438, 137205. DOI: https://doi.org/10.1016/j.conbuildmat.2024.137205

[4] J. Tian, X. Wu, X. Tan, W.-W. Wang, S. Hu, Y. Du, J. Yuan, W. Huang, X. Huang. (2022).

Experimental study and analysis model of flexural synergistic effect of reinforced concrete beams strengthened with ECC. *Construction and Building Materials*, 352, 128987. DOI: https://doi.org/10.1016/j.conbuildmat.2022.128987

[5] P. Jun, V. Mechtcherine. (2010). Behaviour of strain-hardening cement-based composites (SHCC) under monotonic and cyclic tensile loading: part 1–experimental investigations. *Cement and Concrete Composites*, 32(10), 801-809. DOI: https://doi.org/10.1016/j.cemconcomp.2010.07.019

[6] V.C. Li, D.K. Mishra, A.E. Naaman, J.K. Wight, J.M. LaFave, H.-C. Wu, Y. Inada. (1994). On the shear behavior of engineered cementitious composites. *Advanced Cement Based Materials*, 1(3), 142-149. DOI: https://doi.org/10.1016/1065-7355(94)90045-0

[7] K. Yu, Y. Wang, J. Yu, S. Xu. (2017). A strain-hardening cementitious composites with the tensile capacity up to 8%. *Construction and Building Materials*, 137, 410-419. DOI: https://doi.org/10.1016/j.conbuildmat.2017.01.060

[8] C.-L. Nguyen, C.-K. Lee. (2021). Flexural behaviours of Engineered Cementitious Composites–High strength steel composite beams. *Engineering Structures*, 249, 113324. DOI: https://doi.org/10.1016/j.engstruct.2021.113324

[9] K. Yu, L. Li, J. Yu, Y. Wang, J. Ye, Q. Xu. (2018). Direct tensile properties of engineered cementitious composites: A review. *Construction and Building Materials*, 165, 346-362. DOI: https://doi.org/10.1016/j.conbuildmat.2017.12.124

[10] T. Kanda, S. Nagai, M. Maruta, Y. Yamamoto. (2011). New high-rise R/C structure using ECC coupling beams. *2nd International RILEM Conference on Strain Hardening Cementitious Composites (pp. 289-296). RILEM Publications SARL.*

[11] R. Zhang, K. Matsumoto, T. Hirata, Y. Ishizeki, J. Niwa. (2015). Application of PP-ECC in beam–column joint connections of rigid-framed railway bridges to reduce transverse reinforcements. *Engineering Structures*, 86, 146-156. DOI: https://doi.org/10.1016/j.engstruct.2015.01.005

[12] C.-C. Hung, H.-J. Hsiao, Y. Shao, C.-H. Yen. (2023). A comparative study on the seismic performance of RC beam-column joints retrofitted by ECC, FRP, and concrete jacketing methods. *Journal of Building Engineering*, 64, 105691. DOI: https://doi.org/10.1016/j.jobe.2022.105691

[13] X. Yang, L. Xu, J. Pan. (2021). Mechanical behavior of full-scale composite steel plate shear wall restrained by ECC panels. *Journal of Building Engineering*, 44, 102864. DOI: https://doi.org/10.1016/j.jobe.2021.102864

[14] M.K. Ismail, A.A.A. Hassan. (2021). Influence of fibre type on the shear behaviour of engineered cementitious composite beams. *Magazine of Concrete Research*, 73(9), 464-475. DOI: https://doi.org/10.1680/jmacr.19.00172

[15] D. Gu, J. Pan, S. Mustafa, Y. Huang, M. Luković. (2022). Shear transfer mechanism in reinforced engineered cementitious composite (ECC) beams: Quantification of Vs and Vc. *Engineering Structures*, 261, 114282. DOI: https://doi.org/10.1016/j.engstruct.2022.114282

[16] D. Meng, C.K. Lee, Y.X. Zhang. (2017). Flexural and shear behaviours of plain and reinforced polyvinyl alcohol-engineered cementitious composite beams. *Engineering Structures*, 151, 261-272. DOI: https://doi.org/10.1016/j.engstruct.2017.08.036

[17] Y.M.S. Ali, X. Wang, Z. Wu, A.M.A. Moussa, (2025). Numerical simulation on the

performance concrete short beams reinforced with BFRP and steel bars. *Structural Concrete*, 26(5), 6619-6637. https://doi.org/10.1002/suco.70201

[18] A. Alyousif, O. Anil, M. Sahmaran, M. Lachemi, G. Yildirim, A.F. Ashour. (2016). Comparison of shear behaviour of engineered cementitious composite and normal concrete beams with different shear span lengths. *Magazine of Concrete Research*, 68(5), 217-228. DOI: https://doi.org/10.1680/jmacr.14.00336

[19] K. Hamsavathi, S.B. Singh, M.V.R. Sivasubramanian. (2025). Numerical Modelling and Shear Capacity of Steel Reinforced ECC Beams with Short Shear Span. *The Indian Concrete Journal, pp. 16-25.*

[20] F. Abed, A. El Refai, S. Abdalla. (2019). Experimental and finite element investigation of the shear performance of BFRP-RC short beams. *Structures*, 20, 689-701. DOI: https://doi.org/10.1016/j.istruc.2019.06.019

[21] D.J. Carreira, K.-H. Chu. (1985). Stress-strain relationship for plain concrete in compression. *ACI Journal Proceedings*, 82(6), 797-804. DOI: 10.14359/10390

[22] D. Meng, T. Huang, Y.X. Zhang, C.K. Lee. (2017). Mechanical behaviour of a polyvinyl alcohol fibre reinforced engineered cementitious composite (PVA-ECC) using local ingredients. *Construction and Building Materials*, 141, 259-270. DOI: https://doi.org/10.1016/j.conbuildmat.2017.02.158

[23] M.M. Rana, C.K. Lee, S. Al-Deen, Y.X. Zhang. (2018). Flexural behaviour of steel composite beams encased by engineered cementitious composites. *Journal of Constructional Steel Research*, 143, 279-290. https://doi.org/10.1016/j.jcsr.2018.01.004

[24] C.-L. Nguyen & C.-K. Lee. (2023). Development of analytical models for predicting the flexural behaviour of engineered cementitious composites–high strength steel composite beams. *Advanced Steel Construction*, 19(3), 197-208. DOI:10.18057/IJASC.2023.19.3.2

[25] A.-D. Mai, C.-K. Lee, C.-L. Nguyen. (2025). Flexural performance of composite beam with high-strength steel girder and ECC slab: A comprehensive parametric study. *Research on Engineering Structures and Materials (RESM)*, 11(3), 1345-1367. https://doi.org/10.17515/resm2025-860ma0502rs

[26] M.I. Kabir, C.K. Lee, M.M. Rana, Y.X. Zhang. (2020). Flexural behaviour of ECC-LWC encased slender high strength steel composite beams. *Journal of Constructional Steel Research*, 173, 106253. https://doi.org/10.1016/j.jcsr.2020.106253

[27] M. Qasim, C.K. Lee, Y.X. Zhang. (2023). Flexural strengthening of reinforced concrete beams using hybrid fibre reinforced engineered cementitious composite. *Engineering Structures*, 284, 115992. DOI: https://doi.org/10.1016/j.engstruct.2023.115992

[28] X. Wu, T.H.-K. Kang, I.B. Mpalla, C.-S. Kim. (2018). Axial load testing of hybrid concrete columns consisting of UHPFRC tube and normal-strength concrete core. *International Journal of Concrete Structures and Materials*, 12, 43. https://doi.org/10.1186/s40069-018-0275-2